Effect of Diaminopropionic Acid (Dap) on the Biophysical Properties of a Modified Synthetic Channel-Forming Peptide

Urska Bukovnik, Monica Sala-Rabanal, Simonne Francis, Shawnalea J. Frazier, Bruce D. Schultz, Colin G. Nichols and John M. Tomich

Published Version Information

Citation: Bukovnik, U., Sala-Rabanal, M., Francis, S., Frazier, S. J., Schultz, B. D., Nichols, C. G., & Tomich, J. M. (2013). Effect of diaminopropionic acid (Dap) on the biophysical properties of a modified synthetic achannel-forming peptide. Molecular Pharmaceutics, 10(10), 3959-3966.

Digital Object Identifier (DOI): 10.1021/mp4002377

Publisher's Link: http://pubs.acs.org/doi/abs/10.1021/mp4002377

Effect of Diaminopropionic acid (Dap) on the Biophysical Properties of a Modified Synthetic Channel-Forming Peptide

Urska Bukovnik[1]*, Monica Sala-Rabanal[3]*, Simonne Francis[3], Shawnalea J. Frazier[1‡], Bruce D. Schultz[2], Colin G. Nichols[3] and John M. Tomich[1†]

Departments of [1]Biochemistry and [2]Anatomy and Physiology, Kansas State University, Manhattan, KS 66506, and [3]Department of Cell Biology and Physiology, and Center for Investigation of Membrane Excitability Diseases, Washington University School of Medicine, St. Louis, MO 63110, USA

*Equal contribution

[‡]Current address: Circuit Therapeutics, 1505 O'Brien Drive, Menlo Park, CA 94025, USA
[†]Correspondence: Kansas State University Department of Biochemistry, 206 Burt Hall, 66506 Manhattan, KS, USA; Tel.: +1 785 532 5956; Fax: +1 785 532 6297; E-mail: jtomich@ksu.edu

Keywords: Channel-forming peptide; ion selectivity; anion channel; chloride channel; diaminopropionic acid; Dap; channel replacement therapy; cystic fibrosis

Abstract

Channel replacement therapy, based on synthetic channel-forming peptides (CFPs) with the ability to supersede defective endogenous ion channels, is a novel treatment modality that may augment existing interventions against multiple diseases. Previously, we derived CFPs from the second transmembrane segment of the α-subunit of the glycine receptor, M2GlyR, which forms anionic channels in its native form. Our best candidate, NK_4-M2GlyR T19R, S22W (p22-T19R, S22W), was water-soluble, incorporated into cell membranes and was non-immunogenic, but lacked the structural properties for anion selectivity when assembled into a pore. Further studies suggested that the threonine residues at positions 13, 17 and 20 line the pore of assembled p22-T19R, S22W, and here we used 2, 3-diaminopropionic acid (Dap) substitutions to introduce positive charges to the pore-lining interface of the predicted p22-T19R, S22W channel. Dap-substituted p22-T19R, S22W peptides retained the α-helical secondary structure characteristic of their parent peptide, and induced short-circuit transepithelial currents when exposed to the apical membrane of Madin-Darby canine kidney (MDCK) cells; the sequences containing multiple Dap-substituted residues induced larger currents than the peptides with single or no Dap-substitutions. To gain further insights into the effects of Dap residues on the properties of the putative pore, we performed two-electrode voltage clamp electrophysiology on *Xenopus* oocytes exposed to p22-T19R, S22W or its Dap-modified analogs. We observed that Dap-substituted peptides also induced significantly larger voltage-dependent currents than the parent compound, but there was no apparent change in reversal potential upon replacement of external Na^+, Cl^- or K^+, indicating that these currents remained non-selective. Our results suggest that the introduction of positively charged side chains in predicted pore-lining residues does not improve anion selectivity, but results in higher conductance due most likely to an increase in pore size

caused by a higher oligomerization number . Future modifications should include further charge substitutions and a staggering of pore-lining cationic charges.

Introduction

Cystic fibrosis (CF) is a chronic, autosomal recessive disease caused by mutations in the cystic fibrosis transmembrane conductance regulator (CFTR) protein, a Cl^--selective channel with essential roles in ion exchange in epithelial tissues. Impaired CFTR channel activity leads to the abnormal accumulation of mucus that underlies the clinical manifestations of the disease, such as airway inflammation and infection [1]. A major goal of CF treatment strategies, particularly gene therapy, has been the restoration of CFTR channel activity, but none of the methods developed so far have been successful in treating all of the genotypes [2].

A potential alternative may be the use of synthetic channel-forming peptides (CFPs), engineered for high Cl^- selectivity and permeation, in target tissues and organs. CFPs, either designed *de novo* or based on pore-forming transmembrane segments of natural proteins, have been used to generate channel activity in lipid bilayers and cell membranes. Though these CFPs have been shown to assemble into ion-permeable pores, a common limitation has been the lack of combined high conductance and strong selectivity [3-8].

In our studies, the anion-selective pores of native channels, primarily the glycine receptor (GlyR), have been used as templates to synthesize and reconstitute CFPs that form functional synthetic channels in a variety of membrane systems [9-14]. GlyR, a member of the cys-loop super family of ligand-gated channels, is a heteropentameric anion channel formed by three α subunits and two β subunits [15]. The α subunits alone can assemble into homopentameric anionic channels [16], and just the second transmembrane domain (M2) of the α subunit forms

ion channels in lipid bilayers and single cells, and facilitates ion transport across epithelial monolayers [14, 17]. Our founding CFP, M2GlyR, derived from the wild-type α-subunit M2 sequence PARVGLGITTVLTMTTQSSGSRA, conferred net transepithelial ion transport comparable to the parent GlyR channel pore [14], but had poor membrane insertion efficiency and a tendency to aggregate in aqueous solutions [14, 17]. In subsequent studies, modifications were introduced into the amino acid sequence of either the full-length peptide or a truncated version, including a tetralysyl tail at the N-terminus, and the replacement of C-terminal threonine and serine residues with arginine and tryptophan [18-21]. The resulting synthetic peptide KKKKPARVGL-GITTVLTMRTQW, termed NK_4-M2GlyR p22-T19R, S22W (p22-T19R, S22W), demonstrated increased helical content, reduced aggregation, improved efficiency of insertion into epithelial cell membranes, and increased net transepithelial ion conductance in Madin-Darby canine kidney (MDCK) cell monolayers [22]. The p22-T19R, S22W sequence also proved to be non-antigenic in mice at proposed clinical dosages [23], but the putative assembled pore still lacked physiologically relevant anion selectivity [24].

To address these limitations towards the construction of chloride-selective synthetic CFPs with therapeutic potential, we have now tested the possibility that increasing the net positive charge of the pore environment would improve anion selectivity of the predicted p22-T19R, S22W channels. Previous structural analysis suggested that threonine residues at positions 13, 17 and 20 line the pore of hypothetical assembled p22-T19R, S22W channels; in particular, T13 would reside in the widest part, whereas T17 and T20 would be located in the narrowest [20, 25]. Here, we synthesized analogues of p22-T19R, S22W with 2, 3-diaminopropionic acid (Dap) substitutions at T13, T17 and T20 (Table 1), and tested their effect on ion permeation and selectivity, by means of electrophysiological methods in MDCK cells and *Xenopus* oocytes.

Materials and Methods

Chemistry. Peptides were prepared by solid phase (Applied Biosystems Model 431A; Foster City, CA), using 9-fluorenylmethoxycarbonyl (F-moc) chemistry as described [21, 25]; the peptide sequences are shown in Table 1. CLEAR amide resin (0.3 mmol g^{-1}; Peptides International, Louisville, KY) and N^{α}-F-moc amino acids (Anaspec Inc., San Jose, CA) were used. All peptides were purified by HPLC (System Gold HPLC; Beckman Instruments, Inc., Fullerton, CA) with a Phenomenex reversed-phase C-18 column (Torrance, CA), and eluted using a linear gradient of 10-90% acetonitrile containing 0.1% trifluoroacetic acid at 1 ml min^{-1} [26]. Molecular mass was determined by matrix-assisted-laser desorption time-of-flight mass spectroscopy (MALDI-TOF/TOF), using a Bruker Ultraflex II spectrometer (Bruker Daltronics, Billerica, MA). After characterization, peptides were lyophilized and stored as dry powders. Work solutions were prepared immediately before use, and peptide concentrations were determined by measuring the absorbance at 278 nm, using the tryptophan extinction coefficient of 5579 M^{-1} cm^{-1}. The secondary structures of peptides were determined by circular dichroism (CD) at 100 μM in 40% water/trifluoroethanol (TFE), with a J-720 spectropolarimeter (Jasco, Tokyo, Japan), as described [20, 25]. Under the conditions tested, all peptides were in solution as monomers [24].

Transepithelial Electrical Measurements. Madin-Darby canine kidney (MDCK) cells were generously provided by Lawrence Sullivan (Kansas University Medical Center, KS). The cells were cultured in a 1:1 blend of Dulbecco's Modified Eagle Medium and Ham's F-12 Nutrient Mixture (Life Technologies, Carlsbad, CA), supplemented with 5% fetal bovine serum (BioWhittaker, Walkersville, MD) and 10^5 units l^{-1} penicillin/100 mg l^{-1} streptomycin (Life Technologies), and prepared as described [17, 25]. MDCK monolayers were mounted vertically

in DCV9 modified Ussing chambers (Navicyte, San Diego, CA), and the apical and basolateral surfaces were superfused symmetrically with a modified Ringer's solution containing (mM) 120 NaCl, 25 $NaHCO_3$, 3.3 KH_2PO_4, 0.8 K_2HPO_4, 1.2 $MgCl_2$, 1.2 $CaCl_2$ and 10 Hepes/Tris (pH 7.5), kept at 37 °C and bubbled with 5% CO_2. Monolayers with a resistance of at least 800 Ω cm^2 were clamped to 0 mV, and exposed on the apical side to increasing concentrations (10-300 μM) of test peptide. Transepithelial short-circuit current (I_{sc}) was monitored continuously with a custom voltage-clamp setup (Model 558C; University of Iowa Department of Engineering, Iowa City, IA), and 3.2.6 AcqKnowledge software (BIOPAC Systems, Santa Barbara, CA) with an MP100-CE interface was used for data acquisition. I_{sc} data were fitted by Equation 1, for which I_{max} is the derived maximum current, P is the peptide concentration, $K_{0.5}$ is the peptide concentration at which I_{sc} is half-maximal, and n_H is the Hill cooperativity coefficient:

$$I_{sc} = I_{max} P^{n_H} / K_{0.5}^{n_H} + P^{n_H} \quad (1)$$

Two-Electrode Voltage-Clamp Electrophysiology. Mature female *Xenopus laevis* were purchased from Nasco (Fort Atkinson, WI). All animal protocols followed guidelines approved by Washington University and the National Institutes of Health. Frogs were anaesthetized with 0.1% Tricaine (Sigma Chemical Co., Saint Louis, MO) buffered with 0.1% $NaHCO_3$, a portion of the ovary was surgically removed, and the frogs were humanely sacrificed after the final collection. Oocytes were defolliculated by treatment with 0.5 mg ml^{-1} collagenase (Type 1A) in a Ca^{2+}-free solution containing (mM) 82.5 NaCl, 2 KCl, 1 $MgCl_2$, 5 Hepes/Tris (pH 7.5). Stage V-VI oocytes were selected and maintained at 18 °C in modified Barth's solution, supplemented with antibiotics [27], and used up to three days after preparation. Two-microelectrode voltage-clamp (TEVC) was used to determine the response of oocytes to exposure to the peptide in different ionic environments. The standard extracellular solution, ND96, was (mM) 96 NaCl, 1

KCl, 1 $MgCl_2$, 1.8 $CaCl_2$, and 5 Hepes/Tris (pH 7.5). Typically, an oocyte was mounted in the TEVC setup, superfused in ND96 solution and held at –30 mV (V_h). In basic experiments, the oocyte was exposed to ND96, first in absence, then in presence of synthetic peptide (50 μM), and then washed with peptide-free ND96 until the initial conditions were completely restored. In further experiments, the oocyte was first stabilized in ND96, subsequently superfused with the appropriate ion-substituted buffer, first in absence and then in presence of the peptide; after exposure, the oocyte was washed, first with the alternate solution, and then with ND96, to verify the reversibility of bath composition-induced changes. The ion-substituted buffers contained (mM) 96 KCl, 1 NaCl (KD96); 92.3 Na-gluconate, 9.6 NaCl, 1 KCl (Na-Gluc); or 96 K-gluconate, 1 Na-gluconate (K-Gluc); and 5 Hepes/Tris (pH 7.5), plus the appropriate amounts of $CaCl_2$ and $MgCl_2$ to attain constant free Ca^{2+} and Mg^{2+} concentrations, as calculated by means of the CaBuf program (ftp://ftp.cc.kuleuven.ac.be/pub/droogmans/cabuf.zip). At the end of each exposure period, a pulse protocol was applied in which membrane potential (V_m) of oocytes was stepped from V_h to a test value for 1000 ms before returning to V_h. The test potential varied from +60 to −120 mV in 20 mV increments. Steady-state or pseudo steady-state currents were measured at the end of 1000 ms. The reversal potential (V_{rev}) of the current was estimated as the intercept of the linear current-voltage (*I-V*) relationships between +20 and –60 mV. pClamp and Axoscope software (Molecular Devices, Union City, CA) were used for pulse protocol application and data acquisition. All experiments were carried out at room temperature. Unless otherwise noted, experiments were performed in at least three oocytes from different donor frogs.

Data Analysis. Results were analyzed using Excel (Microsoft, Redmond, WA) and Clampfit 10.1 (Molecular Devices). SigmaPlot 10.0 (Systat Software, San Jose, CA) and CorelDRAW X3

13.0 (Corel Corporation, Mountain View, CA) were used for curve fitting, statistics, and figure preparation. Unless otherwise indicated, results are presented as mean ± S.E.M. (standard error of the mean). Where indicated, unpaired Student's *t* test was applied to evaluate statistical differences between groups.

Results and Discussion

Overall Secondary Structure Characteristics. Our model for the NK_4-M2GlyR p22-T19R, S22W (p22-T19R, S22W) pentameric channel suggests that the pore interface is lined by three stacked rings of five threonines, respectively in positions 13, 17 and 20; the T17 and T20 rings form the narrowest part of the pore, whereas the T13 ring defines the widest opening [20, 25]. In an attempt to modify the pore electrostatics to increase the conductance and improve the selectivity of the assembled channel, we designed and synthesized a series of novel p22-T19R, S22W analogues, where T13, T17 or T20 were replaced with positively charged 2, 3-diaminopropionic acid (Dap), a non-natural amino acid that will introduce a methylamine side chain. The sequences and molecular weights of the wild-type (WT) and Dap-substituted peptides are shown in Table 1. By means of circular dichroism (CD) analysis, we confirmed that the introduction of single or multiple Dap substitutions did not significantly alter the secondary structure of the analogues (Figure 1). The CD spectra measured for the WT and Dap-substituted analogues indicated similar helical content, with characteristic α-helix double minima at 208 and 222 nm, and maximum at ~192 nm. These results indicate that the replacement of T13, T17 or T20 with the cationic Dap residue does not affect the propensity of the peptides to adopt a helical conformation in a hydrophobic environment, in agreement with secondary structures determined in previous studies [20, 22, 25].

Electrophysiological Measurements of Transepithelial Conductance. We tested the effect of the peptides on the electrical properties of MDCK cells mounted in Ussing chambers. Figure 2A shows a representative experiment, in which MDCK cell monolayers clamped to 0 mV were exposed to 10-300 μM of p22-T19R, S22W (WT), or analogues with one, two, or three Dap substitutions, and the transepithelial short-circuit current (I_{sc}) response was recorded. Dose-response data were fitted by Equation 1 to estimate the kinetic parameters of peptide-induced transepithelial ion transport, and results are shown in Figure 2B and Table 2. In the presence of the WT peptide, the derived current maximum (I_{max}) was 52 ± 10 μA cm^{-2} (Figure 2B, *black bar*), and the apparent half-saturation constant ($K_{0.5}$) was 195 ± 42 μM (Table 2) (means ± S.E.M. of 6 experiments). For all test peptides, the Hill coefficient (n_H) was greater than 1 (Table 2), suggesting positive cooperativity in the mechanism of action. Furthermore, n_H was ~2 for the WT sequence and up to two fold higher for the Dap analogues (Table 2), and this was reflected in a ~2 to ~2.5-fold increase in I_{max} in cells exposed to Dap17, all three doubly-substituted compounds, and Dap13,17,20 (Figure 2B). No significant differences in $K_{0.5}$ were found between the WT and the Dap-substituted compounds (Table 2).

Voltage-Clamp Characterization of Peptide-Induced Currents. Next, we examined the voltage-dependence and the ion selectivity of the conductances activated by the different test peptides, by means of two-electrode voltage-clamp electrophysiology in *Xenopus* oocytes; results are summarized in Figures 3 and 4, and Table 3. Whole cell currents were recorded in response to 1-s voltage steps between +60 and –120 mV from a holding potential (V_h) of –30 mV (Figure 3A, *upper left panel*), with a 10-s interval between pulses. As exemplified in Figure 3A, oocytes superfused with standard ND96, high K^+ (KD96) or low Cl^- (Na-Gluc) solution showed small leak currents (slope conductance, ~1-2 μS), which reversed at –35 mV (ND96), –3 mV

(KD96), and –39 mV (Na-Gluc), respectively (Figure 3B and Table 3). In low extracellular Na^+ and Cl^- (K-Gluc), the leak conductance increased (~15 µS), and the now clearly sigmoidal current-voltage (*I-V*) relationships reversed at –13 mV (Figure 3B and Table 3). When the oocytes were superfused in ND96 or KD96 in the presence of p22-T19R, S22W (WT), modest outward currents at depolarizing potentials above +20 mV, and larger, slowly-activating, slowly-deactivating inward currents at hyperpolarizing potentials below –80 mV, were evoked. These currents disappeared upon superfusion with peptide-free solution (Figure 3A). In Na-Gluc, exposure to WT led to the activation of fully reversible, outwardly rectifying currents (Figure 3A and 3C). In oocytes superfused with K-Gluc, the amplitude of the currents increased in presence of WT (Figure 3A), but the overall shape of the *I-V* curve remained unchanged (Figure 3C). In all experimental conditions, the WT peptide had a negligible effect on the V_{rev} (Figure 3C and Table 3), indicating that the peptide-activated currents were non-selective.

The substitution of Dap for putative pore-lining threonines led to an increase in conductance, but did not modify the ionic selectivity of the induced currents (Figure 4 and Table 3). As exemplified for ND96 (Figure 4A) and Na-Gluc (Figure 4B), the currents evoked by the Dap-substituted analogues in all solutions were larger but showed similar voltage dependence than those induced by the WT peptide, and again no relevant changes in V_{rev} were observed (Table 3). As summarized in Figure 4C for the net peptide-induced currents measured at +60 mV (outward; *top*) and –100 mV (inward; *bottom*), the increase in current density with respect to the WT sequence was substantial (for example, up to 30-fold in presence of extracellular gluconate) but overall was similar for all Dap-substituted analogues, and there were no evident synergistic or antagonistic effects betwen the different substitutions.

M2GlyR-Derived Channel-Forming Peptides. As part of an ongoing effort to produce synthetic channel forming peptides (CFPs) as potential therapeutics for channel-based diseases, in previous studies we identified p22-T19R, S22W [22-24], a candidate single-spanning membrane protein based on the second transmembrane domain of the glycine receptor (GlyR) α subunit, M2GlyR, which lines the pore of a chloride-selective channel [14, 17]. p22-T19R, S22W showed desirable properties, such as optimal helical content, minimal aggregation in aqueous solutions, enhanced efficiency of membrane insertion and increased induction of ion transport across epithelial cell monolayers [22], and was not immunogenic [23]. However, the hypothetical assembled pore demonstrated only minimal selectivity for monovalent anions over monovalent cations, and relatively low conductance [24], In a further study, we set out to identify relevant pore-lining residues that might be modified to rectify this limitation [25]. Structural analysis, computational modeling and functional assays in MDCK cells, all suggested that the narrowest opening of the putative pentameric assembly is defined by two stacked rings of threonines in positions 17 and 20, whereas the ring of threonines in position 13 forms the widest part [25].

Because electrostatic interactions and the formation of hydrogen bonds within the channel cavity are key determinants of ionic selectivity [28, 29], in the present work we replaced the predicted pore-lining residues T13, T17 and T20 of p22-T19R, S22W with the non-natural diaminopropionic acid (Dap), which carries a net positive charge at physiological pH and can potentially form strong hydrogen bonds with Cl^- ions. Preliminary computer modeling simulations, in which we employed the potential of mean force function [30] to estimate the energy required to move different ions across the simulated Dap-substituted channels, suggested that the introduction of Dap residues to form rings of positive charge in positions 13, 17 and 20

would yield enhanced Cl^- versus Na^+ selectivity. The resulting synthetic Dap-substituted analogues (Table 1) had the appropriate solubility and helical content (Figure 1), and were subsequently used in functional assays to determine their electrogenic properties (Figures 2, 3 and 4, and Tables 2 and 3).

Compared to the WT sequence, transepithelial ion transport rates increased significantly in MDCK cell monolayers exposed to Dap17, to the triply-substituted analogues, and to Dap13,17,20 (Figure 2). For these, the derived Hill coefficient (n_H) was up to 2-fold higher than for the WT (Table 2), suggesting enhanced cooperativity in their function. In *Xenopus* oocytes, voltage-dependent currents induced by the Dap-substituted peptides (Figure 4) were also larger than those evoked by the WT peptide (Figures 3 and 4). However, replacement of extracellular Na^+ with K^+, or Cl^- with gluconate$^-$, did not change the V_{rev} in any case (Table 3), suggesting that, in all cases, the conductance pathway activated by the peptides was non-selective. Nevertheless, it is intriguing, and important for the ultimate therapeutic potential of our CFPs, that the induced conductances consistently increased with the introduction of positive charges. This might reflect the Dap-substituted peptides associating in entities of a higher order than the pentameric assembly predicted for the parent sequence [20, 24, 25], consistent with reports of variable conductances associated to different aggregation states of channel subunits [31]. Further charge substitutions should be considered for future modifications.

Acknowledgements We thank Dr. Yasuaki Hiromasa (KSU) for the MS measurements. This is publication 13-311-J from the Kansas Agricultural Experiment Station. Partial support for this project was provided by PHS-NIH grant # RO1 GM074096 (to J.M.T) and the Terry Johnson Cancer Center for summer support (for U.B.)

References

[1] T.S. Cohen, A. Prince, Cystic fibrosis: a mucosal immunodeficiency syndrome, Nat Med, 18 (2012) 509-519.
[2] F. Becq, Cystic fibrosis transmembrane conductance regulator modulators for personalized drug treatment of cystic fibrosis: progress to date, Drugs, 70 (2010) 241-259.
[3] E. Abel, G.E.M. Maguire, E.S. Meadows, O. Murillo, T. Jin, G.W. Gokel, Planar bilayer conductance and fluorescence studies confirm the function and location of a synthetic, sodium-ion-conducting channel in a phospholipid bilayer membrane, Journal of the American Chemical Society, 119 (1997) 9061-9062.
[4] Y. Agawa, S. Lee, S. Ono, H. Aoyagi, M. Ohno, T. Taniguchi, K. Anzai, Y. Kirino, Interaction with phospholipid bilayers, ion channel formation, and antimicrobial activity of basic amphipathic alpha-helical model peptides of various chain lengths, The Journal of biological chemistry, 266 (1991) 20218-20222.
[5] C. Krittanai, S. Panyim, Structural design and characterization of a channel-forming peptide, Journal of Biochemistry and Molecular Biology, 37 (2004) 460-465.
[6] S. Oiki, W. Danho, M. Montal, Channel protein engineering: synthetic 22-mer peptide from the primary structure of the voltage-sensitive sodium channel forms ionic channels in lipid bilayers, Proceedings of the National Academy of Sciences of the United States of America, 85 (1988) 2393-2397.
[7] R. Pajewski, R. Garcia-Medina, S.L. Brody, W.M. Leevy, P.H. Schlesinger, G.W. Gokel, A synthetic, chloride-selective channel that alters chloride transport in epithelial cells, Chem Commun (Camb), (2006) 329-331.
[8] M.T. Tosteson, D.S. Auld, D.C. Tosteson, Voltage-gated channels formed in lipid bilayers by a positively charged segment of the Na-channel polypeptide, Proceedings of the National Academy of Sciences of the United States of America, 86 (1989) 707-710.
[9] T. Iwamoto, A. Grove, M.O. Montal, M. Montal, J.M. Tomich, Chemical synthesis and characterization of peptides and oligomeric proteins designed to form transmembrane ion channels, Int J Pept Protein Res, 43 (1994) 597-607.
[10] M. Montal, M.S. Montal, J.M. Tomich, Synporins--synthetic proteins that emulate the pore structure of biological ionic channels, Proceedings of the National Academy of Sciences of the United States of America, 87 (1990) 6929-6933.
[11] M.O. Montal, T. Iwamoto, J.M. Tomich, M. Montal, Design, synthesis and functional characterization of a pentameric channel protein that mimics the presumed pore structure of the nicotinic cholinergic receptor, FEBS letters, 320 (1993) 261-266.
[12] M. Oblatt-Montal, L.K. Buhler, T. Iwamoto, J.M. Tomich, M. Montal, Synthetic peptides and four-helix bundle proteins as model systems for the pore-forming structure of channel proteins. I. Transmembrane segment M2 of the nicotinic cholinergic receptor channel is a key pore-lining structure, The Journal of biological chemistry, 268 (1993) 14601-14607.
[13] M. Oblatt-Montal, G.L. Reddy, T. Iwamoto, J.M. Tomich, M. Montal, Identification of an ion channel-forming motif in the primary structure of CFTR, the cystic fibrosis chloride channel, Proceedings of the National Academy of Sciences of the United States of America, 91 (1994) 1495-1499.
[14] G.L. Reddy, T. Iwamoto, J.M. Tomich, M. Montal, Synthetic peptides and four-helix bundle proteins as model systems for the pore-forming structure of channel proteins. II. Transmembrane

segment M2 of the brain glycine receptor is a plausible candidate for the pore-lining structure, The Journal of biological chemistry, 268 (1993) 14608-14615.
[15] M. Cascio, Structure and function of the glycine receptor and related nicotinicoid receptors, The Journal of biological chemistry, 279 (2004) 19383-19386.
[16] V. Schmieden, G. Grenningloh, P.R. Schofield, H. Betz, Functional expression in Xenopus oocytes of the strychnine binding 48 kd subunit of the glycine receptor, EMBO J, 8 (1989) 695-700.
[17] D.P. Wallace, J.M. Tomich, T. Iwamoto, K. Henderson, J.J. Grantham, L.P. Sullivan, A synthetic peptide derived from glycine-gated Cl- channel induces transepithelial Cl- and fluid secretion, The American journal of physiology, 272 (1997) C1672-1679.
[18] J.R. Broughman, K.E. Mitchell, R.L. Sedlacek, T. Iwamoto, J.M. Tomich, B.D. Schultz, NH(2)-terminal modification of a channel-forming peptide increases capacity for epithelial anion secretion, American journal of physiology. Cell physiology, 280 (2001) C451-458.
[19] J.R. Broughman, L.P. Shank, O. Prakash, B.D. Schultz, T. Iwamoto, J.M. Tomich, K. Mitchell, Structural implications of placing cationic residues at either the NH2- or COOH-terminus in a pore-forming synthetic peptide, The Journal of membrane biology, 190 (2002) 93-103.
[20] G.A. Cook, O. Prakash, K. Zhang, L.P. Shank, W.A. Takeguchi, A. Robbins, Y.X. Gong, T. Iwamoto, B.D. Schultz, J.M. Tomich, Activity and structural comparisons of solution associating and monomeric channel-forming peptides derived from the glycine receptor m2 segment, Biophys J, 86 (2004) 1424-1435.
[21] J.M. Tomich, D. Wallace, K. Henderson, K.E. Mitchell, G. Radke, R. Brandt, C.A. Ambler, A.J. Scott, J. Grantham, L. Sullivan, T. Iwamoto, Aqueous solubilization of transmembrane peptide sequences with retention of membrane insertion and function, Biophys J, 74 (1998) 256-267.
[22] L.P. Shank, J.R. Broughman, W. Takeguchi, G. Cook, A.S. Robbins, L. Hahn, G. Radke, T. Iwamoto, B.D. Schultz, J.M. Tomich, Redesigning channel-forming peptides: amino acid substitutions that enhance rates of supramolecular self-assembly and raise ion transport activity, Biophys J, 90 (2006) 2138-2150.
[23] F.W. van Ginkel, T. Iwamoto, B.D. Schultz, J.M. Tomich, Immunity to a self-derived, channel-forming peptide in the respiratory tract, Clin Vaccine Immunol, 15 (2008) 260-266.
[24] A.I. Herrera, A. Al-Rawi, G.A. Cook, J. Gao, T. Iwamoto, O. Prakash, J.M. Tomich, J. Chen, Structural characterization of two pore-forming peptides: consequences of introducing a C-terminal tryptophan, Proteins, 78 (2010) 2238-2250.
[25] U. Bukovnik, J. Gao, G.A. Cook, L.P. Shank, M.B. Seabra, B.D. Schultz, T. Iwamoto, J. Chen, J.M. Tomich, Structural and biophysical properties of a synthetic channel-forming peptide: Designing a clinically relevant anion selective pore, Biochimica et biophysica acta, 1818 (2012) 1039-1048.
[26] I. Ivanov, X. Cheng, S.M. Sine, J.A. McCammon, Barriers to ion translocation in cationic and anionic receptors from the Cys-loop family, J Am Chem Soc, 129 (2007) 8217-8224.
[27] M. Sala-Rabanal, D.C. Li, G.R. Dake, H.T. Kurata, M. Inyushin, S.N. Skatchkov, C.G. Nichols, Polyamine Transport by the Polyspecific Organic Cation Transporters OCT1, OCT2, and OCT3, Molecular pharmaceutics, (2013).
[28] D. Bichet, M. Grabe, Y.N. Jan, L.Y. Jan, Electrostatic interactions in the channel cavity as an important determinant of potassium channel selectivity, Proceedings of the National Academy of Sciences of the United States of America, 103 (2006) 14355-14360.

[29] R. Dutzler, E.B. Campbell, R. MacKinnon, Gating the selectivity filter in ClC chloride channels, Science, 300 (2003) 108-112.
[30] T.W. Allen, O.S. Andersen, B. Roux, Molecular dynamics - potential of mean force calculations as a tool for understanding ion permeation and selectivity in narrow channels, Biophysical chemistry, 124 (2006) 251-267.
[31] M.C. Lin, B.L. Kagan, Electrophysiologic properties of channels induced by Abeta25-35 in planar lipid bilayers, Peptides, 23 (2002) 1215-1228.

Table 1. Sequences of NK_4-M2GlyR p22-T19R, S22W (p22-T19R, S22W) and Dap-substituted peptides. Abbreviations used in the text are shown in parentheses.

Peptide ID	Sequence	g mol^{-1}
p22-T19R, S22W (WT)[22]	$(K)_4$PARVGLGITTVLTMRTQW	2512.1
p22-T19R, S22W, T13Dap (Dap13)	$(K)_4$PARVGLGI**Dap**TVLTMRTQW	2497.1
p22-T19R, S22W, T17Dap (Dap17)	$(K)_4$PARVGLGITTVL**Dap**MRTQW	2497.1
p22-T19R, S22W, T20Dap (Dap20)	$(K)_4$PARVGLGITTVLTMR**Dap**QW	2497.1
p22-T19R, S22W, T13Dap, T17Dap (Dap13,17)	$(K)_4$PARVGLGI**Dap**TVL**Dap**MRTQW	2482.1
p22-T19R, S22W, T13Dap, T20Dap (Dap13,20)	$(K)_4$PARVGLGI**Dap**TVLTMR**Dap**QW	2482.1
p22-T19R, S22W, T17Dap, T20Dap (Dap17,20)	$(K)_4$PARVGLGITTVL**Dap**MR**Dap**QW	2482.1
p22-T19R, S22W, T13Dap, T17Dap, T20Dap (Dap13,17,20)	$(K)_4$PARVGLGI**Dap**TVL**Dap**MR**Dap**QW	2467.1

Table 2. Kinetics of short-circuit currents in MDKC cells exposed to p22-T19R, S22W (WT) and Dap-substituted analogs. Dose-response I_{sc} data were fitted by Equation 1 to estimate the maximum current (I_{max}, Fig. 2), the peptide concentration for half-maximal I_{sc} ($K_{0.5}$), and the Hill cooperativity coefficient (n_H) of peptide-induced transepithelial ion transport. Data are from the same experiments as in Figure 2. Results are means ± S.E.M. of 4–6 experiments. ***** $p < 0.05$ as compared to the WT sequence (unpaired Student's *t* test).

Peptide ID	n_H	$K_{0.5}$ **(μM)**
WT	1.8 ± 0.3	195 ± 42
Dap13	3.3 ± 0.5*	161 ± 22
Dap17	2.6 ± 0.1*	198 ± 50
Dap20	2.5 ± 0.5	145 ± 24
Dap13,17	2.7 ± 0.3	160 ± 20
Dap13,20	3.4 ± 0.4*	140 ± 16
Dap17,20	3.8 ± 0.4*	105 ± 7
Dap13,17,20	3.2 ± 0.7	129 ± 20

Table 3. Reversal potential (V_{rev}) of currents recorded in *Xenopus* oocytes superfused with the different experimental buffers, and changes in V_{rev} (ΔV_{rev}) induced by exposure to NK_4-M2GlyR p22-T19R, S22W (p22-T19R, S22W) or Dap-substituted peptides. Oocytes were held at –30 mV and stepped to test values (+60 to −120 mV, in 20 mV increments), and steady-state or pseudo steady-state currents were measured at the end of each 1000-ms voltage step. V_{rev} was estimated as the intercept of linear *I-V* relationships between +20 and –60 mV. Data are from the same experiments as in Figures 3 and 4. Results are means ± S.E.M. of 3–8 experiments.

	ND96	**KD96**	**Na-Gluc**	**K-Gluc**
In absence of peptide		**V_{rev} (mV)**		
	–35 ± 3	–3 ± 5	–39 ± 4	–14 ± 2
In presence of peptide		**ΔV_{rev} (mV)**		
WT	4 ± 2	2 ± 1	4 ± 1	6 ± 1
Dap13	2 ± 3	8 ± 3	3 ± 2	6 ± 1
Dap17	5 ± 2	2 ± 2	6 ± 3	9 ± 3
Dap20	5 ± 3	6 ± 1	1 ± 1	6 ± 2
Dap13,17	5 ± 1	5 ± 3	5 ± 4	7 ± 3
Dap13,20	3 ± 2	6 ± 1	6 ± 1	3 ± 1
Dap17,20	5 ± 2	5 ± 3	7 ± 1	4 ± 1
Dap13,17,20	5 ± 4	4 ± 1	4 ± 2	5 ± 2

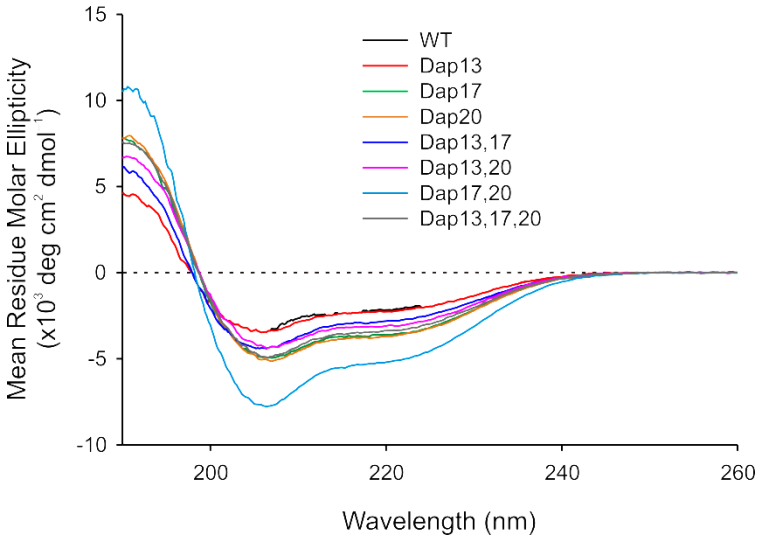

Figure 1. Circular dichroism spectra of p22-T19R, S22W (WT) and Dap-substituted analogs. Peptides were reconstituted to 100 µM in 40% water/TFE, and spectra were recorded at 25 °C (Neslab RTE-IIM circulator; Thermo Scientific, Waltham, MA). Data are the averages of five scans, after background subtraction.

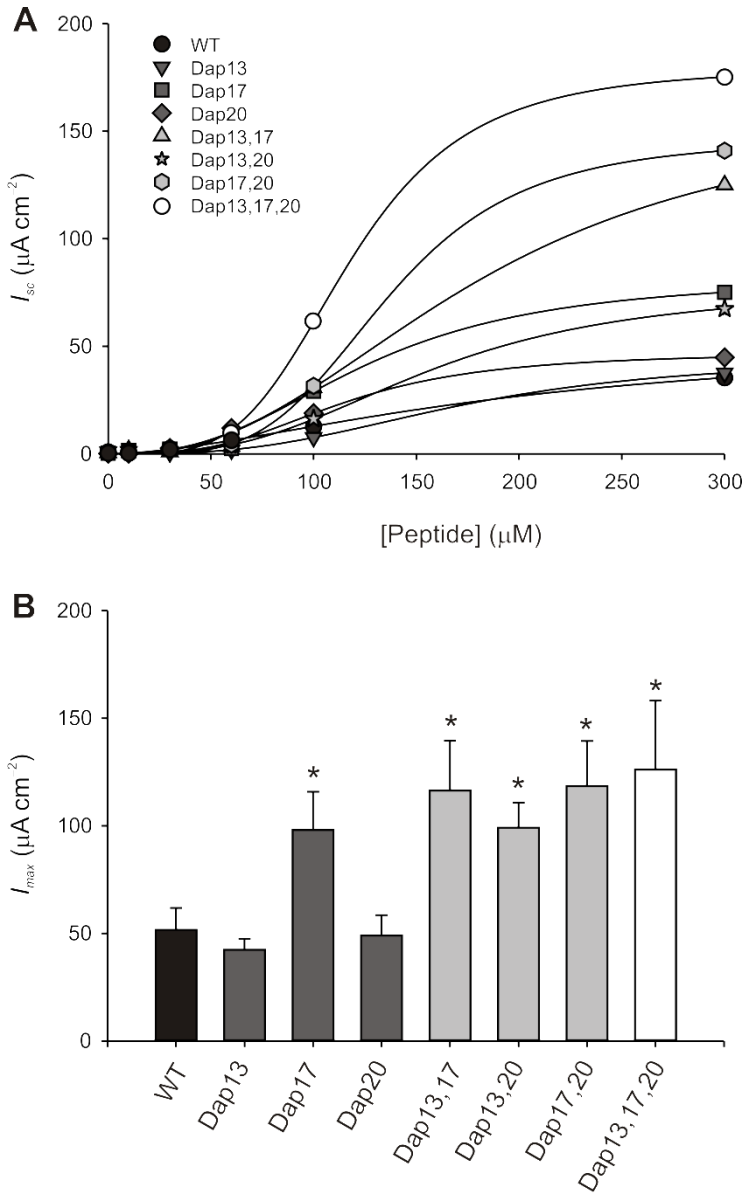

Figure 2. Concentration-dependence of short-circuit currents (I_{sc}) induced by p22-T19R, S22W and Dap-substituted peptides in MDCK cells. ***A***, representative experiment. MDCK monolayers mounted in Ussing chambers were clamped to 0 mV, and transepithelial I_{sc} were measured in presence of increasing concentrations of p22-T19R, S22W (WT, *black symbols*) or analog peptides with one (*dark gray*), two (*light gray*) or three (*white*) Dap-substituted residues. *Lines*, I_{sc} data were fitted by Equation 1 to estimate the kinetic parameters of peptide-induced transepithelial ion transport; current maxima (I_{max}) are summarized in ***B***, and the peptide concentration for half-maximal I_{sc} ($K_{0.5}$) and Hill cooperativity coefficient (n_H) values are shown in Table 2. *B*, Results are means ± S.E.M. of 4–6 experiments. *****$p < 0.05$ as compared to the WT sequence (unpaired Student's *t* test).

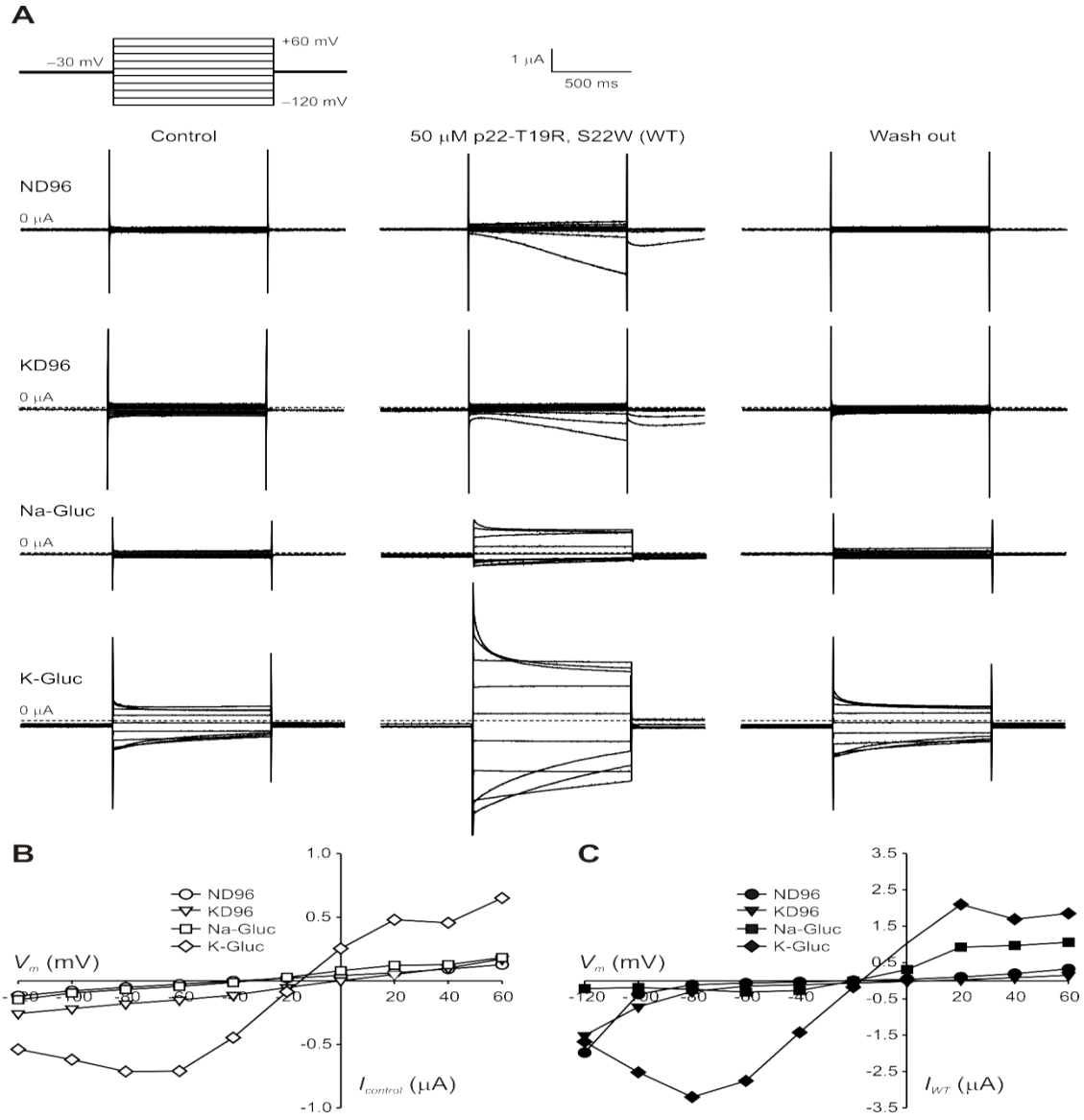

Figure 3. Voltage dependence of currents measured in *Xenopus* oocytes. *A*, representative experiments. Oocytes were superfused with ND96 or the appropriate ion-substituted solution, first in absence (*control*), then in presence of 50 μM p22-T19R, S22W (WT), and again in the absence of peptide (*wash out*). Currents were recorded as the membrane potential was held at –30 mV and stepped to test values, as in the pulse protocol shown in the upper left panel. The dotted lines indicate zero current. ***B–C***, current-voltage (*I-V*) relationships from the oocytes shown in *A*. For each experimental buffer, steady-state or pseudo steady-state currents induced in absence ($I_{control}$; *B*) or presence of peptide (I_{WT}; *C*) were measured at the end of the 1000-ms voltage pulse.

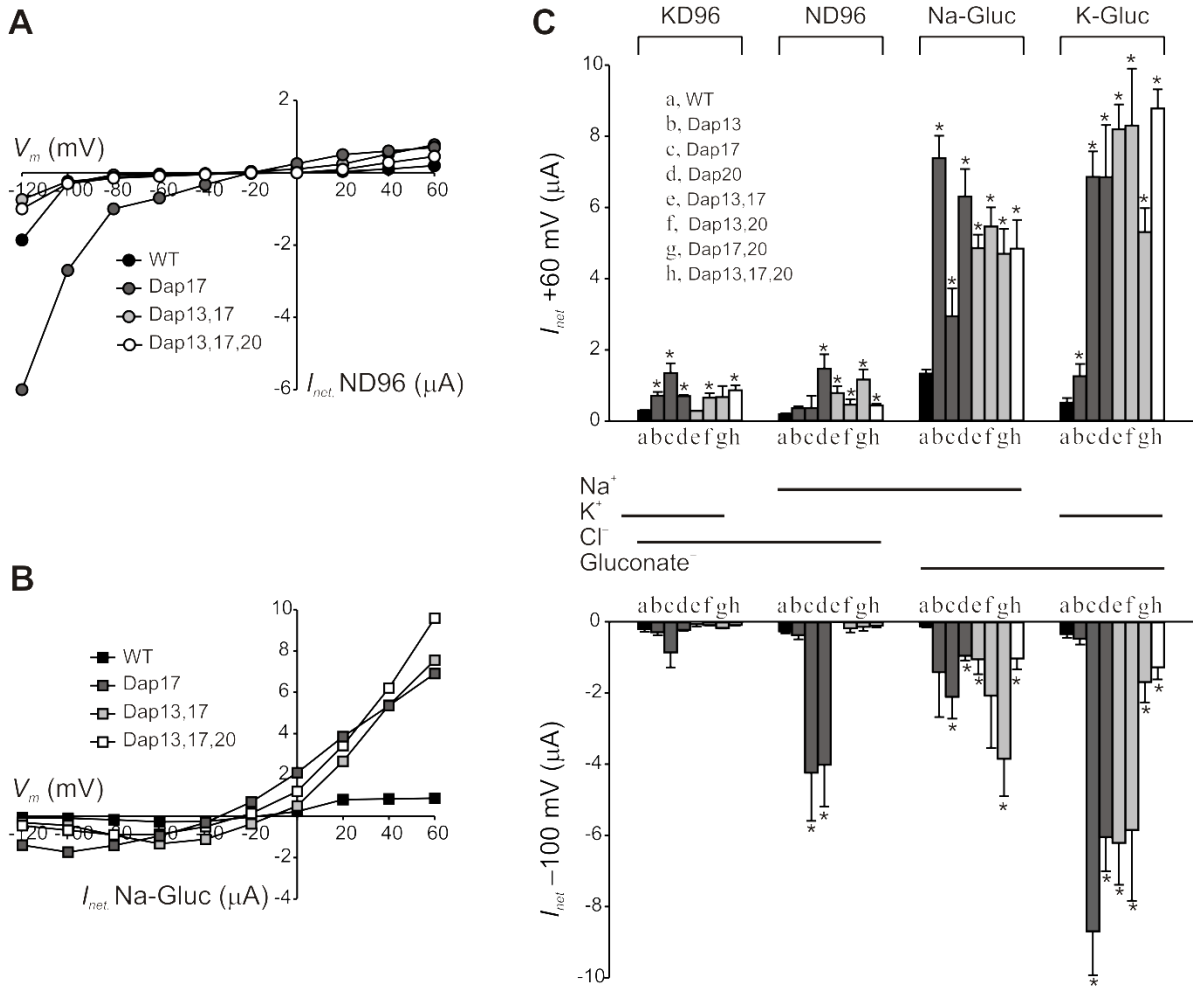

Figure 4. Currents evoked by p22-T19R, S22W and Dap-substituted peptides in *Xenopus* oocytes. Experiments were performed as in Figure 3. Oocytes were exposed to 50 μM WT (*black*) or singly- (*dark gray*), doubly- (*light gray*) or triply- (*white*) Dap-substituted analogues, and the net peptide-induced currents (I_{net}) were calculated by subtracting the total currents from the currents measured in the absence of peptides. ***A–B,*** *I-V* relationships from representative oocytes exposed to WT or selected analogues in ND96 (*A*) or Na-Gluc (*B*) buffer. ***C,*** summary of peptide-induced outward (+60 mV; *top*) and inward (–100 mV; *bottom*) currents measured in the different experimental solutions. The background currents were, at +60 mV (in nA), 245 ± 36 (KD96), 114 ± 10 (ND96), 152 ± 15 (Na-Gluc), and 484 ± 137 (K-Gluc); and at –100 mV (in nA), –257 ± 36 (KD96), –117 ± 16 (ND96), –110 ± 15 (Na-Gluc), and –416 ± 146 (K-Gluc). Results are means ± S.E.M. of 3–8 experiments.*****$p < 0.05$ as compared to the WT sequence (unpaired Student's *t* test).